inorganics

MDPI

Article

Hydrazine Oxidation in Aqueous Solutions I: N_4H_6 Decomposition

Martin Breza [1,*] and Alena Manova [2]

[1] Department of Physical Chemistry, Slovak Technical University, Radlinskeho 9, SK-81237 Bratislava, Slovakia
[2] Department of Analytical Chemistry, Slovak Technical University, Radlinskeho 9, SK-81237 Bratislava, Slovakia; alena.manova@stuba.sk
* Correspondence: martin.breza@stuba.sk

Abstract: A mixture of nonlabeled ($^{14}N_2H_4$) and ^{15}N labeled hydrazine ($^{15}N_2H_4$) in an aqueous solution is oxidized to $^{15}N_2$, $^{14}N_2$, and $^{14}N^{15}N$ molecules, indicating the intermediate existence of the $^{14}NH_2$-^{14}NH-^{15}NH-$^{15}NH_2$ with subsequent hydrogen transfers and splitting of side N-N bonds. The structures, thermodynamics and electron characteristics of various N_4H_6 molecules in aqueous solutions are investigated using theoretical treatment at the CCSD/cc-pVTZ level of theory to explain the crucial part of the hydrazine oxidation reaction. Most N_4H_6 structures in aqueous solutions are decomposed during geometry optimization. Splitting the bond between central nitrogen atoms is the most frequent method, but the breakaway of the side nitrogen is energetically the most preferred one. The N-N fissions are enabled by suitable hydrogen rearrangements. Gibbs free energy data indicate the dominant abundance of NH_3... N_2... NH_3 species. The side N atoms have very high negative charges, which should support hydrogen transfers in aqueous solutions. The only stable cyclo-$(NH)_4$...H_2 structure has a Gibbs energy that is too high and breaks the H_2 molecule. The remaining initial cyclic structures are split into hydrazine and HN≡NH or $H_2N{\equiv}N$ species, and their relative abundance in aqueous solutions is vanishing.

Keywords: Coupled Cluster; geometry optimization; N-N bond splitting; QTAIM analysis; electron structure

Citation: Breza, M.; Manova, A. Hydrazine Oxidation in Aqueous Solutions I: N_4H_6 Decomposition. *Inorganics* **2023**, *11*, 413. https://doi.org/10.3390/inorganics11100413

Academic Editors: Hicham Idriss, Roberto Nisticò, Torben R. Jensen, Luciano Carlos and Eleonora Aneggi

Received: 29 September 2023
Revised: 14 October 2023
Accepted: 17 October 2023
Published: 18 October 2023

1. Introduction

Hydrazine N_2H_4 is a colorless flammable liquid that is used in industry and agriculture due to its reducing properties. It is used as a corrosion inhibitor in boilers, as a rocket propellant, antioxidant, catalyst, and pesticide precursor. In boiler water, it serves as an oxygen scavenger that reacts with oxygen into nitrogen and water only, which does not cause corrosion of ferrous metals. Unreacted hydrazine can be decomposed into ammonia, which can be corrosive to copper and copper-containing alloys [1]. Thus, the knowledge of the exact mechanism of its oxidation is of practical importance so far.

Higginson and Sutton [2] studied the oxidation of ^{15}N-enriched hydrazine by an excess of various oxidizing agents in aqueous solutions. Mass spectroscopic analysis of the evolved nitrogen for 28, 29 and 30 mass-number abundance (i.e., incidence of $^{14}N_2$, $^{15}N^{14}N$ and $^{15}N_2$ molecules, respectively) has shown that the proportion of $^{15}N_2$ molecules decreased while that of $^{15}N^{14}N$ molecules increased depending on the oxidizing agent used. If the nitrogen produced by the reaction

$$2\,N_2H_4 \rightarrow N_2 + 2\,NH_3 \quad (1)$$

involves no N-N fission, the evolved N_2 molecule originates in the same N_2H_4 molecule, and therefore it must have the same distribution of ^{15}N isotopes as the hydrazine reactant. This implies that some of the nitrogen molecules are formed by a mechanism involving a N-N fission and the formation of nitrogen-containing radicals from two different hydrazine molecules as follows:

$$^{15}NH_2\text{-}^{15}NH_2 + {}^{14}NH_2\text{-}^{14}NH_2 \rightarrow {}^{15}NH_2\text{-}^{15}NH\bullet + \bullet{}^{14}NH\text{-}^{14}NH_2 \rightarrow {}^{15}NH_2\text{-}^{15}NH\text{-}^{14}NH\text{-}^{14}NH_2 \quad (2)$$

$$^{15}NH_2\text{-}^{15}NH\text{-}^{14}NH\text{-}^{14}NH_2 \rightarrow {}^{15}NH_3 + {}^{15}NH = {}^{14}N\text{-}^{14}NH_2 \rightarrow {}^{15}NH_3 + {}^{15}N^{14}N + {}^{14}NH_3 \quad (3)$$

$$^{15}NH_2\text{-}^{15}NH\text{-}^{14}NH\text{-}^{14}NH_2 \rightarrow {}^{15}NH_2\text{-}^{15}N = {}^{14}NH + {}^{14}NH_3 \rightarrow {}^{15}NH_3 + {}^{15}N^{14}N + {}^{14}NH_3 \quad (4)$$

Cahn and Powell [3] confirmed the randomized $^{15}N^{14}N$ composition obtained by one-electron oxidation of ^{15}N enriched hydrazines with a number of oxidizing agents unlike exclusively four-electron oxidizing agents (acid iodate, alkaline ferricyanide) that produced unrandomized N_2 molecules (all four hydrogen atoms must be removed from a single hydrazine molecule). Petek and Bruckenstein [4] observed that the electrooxidation of ^{15}N labelled hydrazine (96.7% enrichment) at the Pt electrode produced N_2 molecules with the ratio of $^{14}N^{15}N/^{15}N^{15}N = 0.07 \pm 0.01$ while in Ce(IV) solutions it was 0.9 ± 0.2. A ratio of both isotopic forms between these two limits was produced by simultaneous electrooxidation and homogeneous oxidation with electrogenerated Ce(IV).

A bright yellow substance, stable under −178 °C, is formed after thermal decomposition of hydrazine at high temperatures (~850 °F) and low pressures (~0.5 mm Hg) in a flowing system [5]. The authors suppose that it is tetrazane N_4H_6.

Based on polarographic and voltammetric studies of hydrazine in alkali solutions, Karp and Meites [6] suggested its two-electron oxidation to diimide with subsequent dimerization and decomposition as follows

$$2\ N_2H_2 \rightarrow N_4H_4 \rightarrow NH_4^+ + N_3^- \quad (5)$$

The proposed mechanism is also capable of explaining the randomized $^{15}N^{14}N$ composition.

Ball [7] investigated the structure and some thermochemical properties of the cis- and trans-conformations of tetrazane NH_2-NH-NH-NH_2 using various-level ab initio methods. Unlike nearly planar trans-conformation, the cis-conformation should be denoted as a gauche structure (N-N-N-N dihedral angle of ca 90°).

The decomposition of hydrazine was studied at the CCSD(T)-F12a/aug-ccpVTZ//ωB97x-D3/6-311++G(3df,3pd) level of theory [8]. A comprehensive analysis of the N_4H_6 singlet potential energy surfaces was performed. Three stable isomers, NH_2-NH-NH-NH_2, NH_2-NH-NH_2=NH and NH_2-NH_2-N=NH_2, and the transition states for H transfers between them were obtained as well. Stabilized NH_2-NH-NH-NH_2 formation becomes significant only at relatively high pressures and low temperatures due to its decomposition into $N_2H_3\bullet$ + $N_2H_3\bullet$. No direct reaction between NH_2-NH-NH-NH_2 and NH_2-NH_2-N=NH_2 was found. NH_3 eliminations from NH_2-NH-NH-NH_2 and NH_2-NH_2-N=NH_2 are energetically preferred, but only NH_2-NH_2-N=NH_2 has relatively small activation energy for this reaction (see Table 1).

Table 1. Reaction, ΔE_r, and activation, E_a, energy data from elementary reactions on the N_4H_6 potential energy surface [8].

Reaction	ΔE_r (kJ/mol)	E_a (kJ/mol
$N_2H_4 + H_2N{=}N \rightarrow NH_2$-NH-NH-$NH_2$	−103.6	50.6
$N_2H_4 + H_2N{=}N \rightarrow NH_2NH_2N{=}NH_2$	29.0	55.4
NH_2-NH-NH-$NH_2 \rightarrow NH_2NH{=}N + NH_3$	7.5	178.7
NH_2-NH-NH-$NH_2 \rightarrow NH_2$-N=NH + NH_3	−102.5	214.1
NH_2-NH_2-N=$NH_2 \rightarrow NH_2$-N=NH + NH_3	−245.1	38.7
NH_2-NH-NH-$NH_2 \rightarrow NH_2$-NH-NH_2=NH	151.1	158.6
NH_2-NH-NH_2=NH → NH_2-NH_2-N=NH_2	−18.5	74.4
$N_2H_3\bullet + N_2H_3\bullet \rightarrow NH_2$-NH-NH-$NH_2$	−152.9	0.2
NH_2-NH=NH• + $NH_2\bullet \rightarrow NH_2$-NH-NH-$NH_2$	208.9	0.2
NH=NH_2-NH• + NH2• → NH_2-NH-NH_2=NH	682.7	0.2
NH_2-N=$NH_2\bullet + NH_2\bullet \rightarrow NH_2$-$NH_2$-N=$NH_2$	37.9	2.8

It is evident that the decomposition of N_4H_6 is crucial for hydrazine oxidation with subsequent $^{15}N^{14}N$ molecule formation. It depends on the suitable N_4H_6 site of N-N bond splitting. At first, the NH_2-NH-NH-NH_2 isomer is formed by the reaction

$$N_2H_3\bullet + N_2H_3\bullet \rightarrow NH_2\text{-}NH\text{-}NH\text{-}NH_2 \quad (6)$$

In the next steps, H transfers and possible N-N bond splitting may proceed. The main aim of this study is a quantum-chemical study of N_4H_6 isomers in aqueous solutions solely at the Coupled Cluster level of theory and to determine the sites of the possible N-N fission within them. The thermodynamic properties of the decomposition reaction products enable us to predict the possible formation of $^{15}N^{14}N$ molecules in real systems. The electronic structure of the optimized structures will also be discussed.

2. Results and Discussion

We consider possible linear isomers of N_4H_6 with an N1-N2-N3-N4 backbone and the composition of $N1H_m$-$N2H_n$-$N3H_p$-$N4H_q$, where subscripts m, n, p and q denote the number of H atoms bonded to individual Ni; i = 1→ 4, atoms, and m + n + p + q = 6. We started geometry optimizations from anti- and syn-conformations of N1-N2-N3-N4. The optimized structures usually correspond to gauche conformers, or some N-N bonds are split (see Table 2). If N1 and N2 correspond to ^{15}N atoms, while N3 and N4 correspond to the ^{14}N ones, then N1-N2 and N3-N4 fissions would lead to $^{15}N^{14}N$ molecules, unlike the N2-N3 fissions.

Table 2. N1-N2-N3-N4 dihedral angles (Θ_{1234}), absolute (G_{298}) and relative (ΔG_{298}) Gibbs free energies at 298.15 K for the optimized N_4H_6 structures obtained from the starting ones. The most stable structure is highlighted in bold. The different structures with the same notation are distinguished by additional letters a, b, c, or d.

Starting	Optimized	Θ_{1234} [°]	G_{298} [Hartree]	ΔG_{298} [kJ/mol]	Remarks
A2112	D2112a	168.3	−222.09177	0.00	
A2121	D2121a	−161.4	−222.04654	118.75	
A2211	E(22)(11)a	−33.7	−222.10760	−41.56	$H_2N\text{-}NH_2$ + HN=NH
A2202	A2202	−179.9	−222.04618	119.71	
A2220	E(22)(20)a	146.5	−222.07817	35.7	$H_2N\text{-}NH_2$ + H_2N=N
A1221	D1221	−168.5	−222.00357	231.58	
A3210	E(32)(10)	14.3	−222.04629	119.42	$H_3N\text{-}NH_2$ + HN=N
A3201	E(22)(11)b	−142.8	−222.10755	−41.43	$H_2N\text{-}NH_2$ + HN=NH, 1→3 H rearrangement
A3201	E(3)(201)	−26.5	−222.14890	−150.04	NH_3 + H_2N-N=NH
A3111	D2112b	75.6	−222.09311	−3.52	1→4 H rearrangement
A3120	E(31)(20)	−21.4	−222.03229	156.16	H_3N-NH + H_2N=N
A3102	E(3)(102)a	−177.1	−222.14926	−150.94	NH_3 + HN=N-NH_2
A3012	D3012a	88.8	−222.04832	114.07	
A3021	A3021	176.8	−221.99866	244.46	
A3003	**E(3)(00)(3)**	**60.4**	**−222.26295**	**−449.44**	$2NH_3$ + N_2
B2112	D2112c	72.0	−222.09665	−12.80	
B2121	D2121b	−65.0	−222.04530	122.02	
B2121	D2121c	−44.8	−222.04982	110.13	
B2211	E(22)(11)a	−33.7	−222.10760	−41.56	$H_2N\text{-}NH_2$ + HN=NH
B2202	D2202a	73.7	−222.05056	108.21	
B2220	E(22)(20)b	−32.9	−222.07820	35.64	$H_2N\text{-}NH_2$ + H_2N=N
B1221	F12)(21	75.8	−222.09760	−15.30	N2-N3 fission, N1-N4 bonding
B1221	F1)(22)(1	−33.3	−222.10756	−41.45	$H_2N\text{-}NH_2$ + HN=NH, N1-N4 bonding
B3210	E(22)(11)c	−34.0	−222.10754	−41.41	$H_2N\text{-}NH_2$ + HN=NH, 1→4 H rearrangement
B3201	D2202b	80.1	−222.04758	116.02	1→4 H rearrangement
B3201	E(3)(201)	−26.5	−222.14892	−150.04	NH_3 + H_2N=N-NH
B3111	D2112b	75.6	−222.09311	−3.52	1→4 H rearrangement
B3120	D2121d	68.8	−222.04651	118.82	1→4 H rearrangement
B3102	E(3)(102)b	−20.6	−222.14678	−144.42	NH_3 + HN=N-NH_2

Table 2. *Cont.*

Starting	Optimized	Θ_{1234} [°]	G_{298} [Hartree]	ΔG_{298} [kJ/mol]	Remarks
B3012	D3012b	−59.7	−222.04910	112.02	
B3021	D2022	−73.8	−222.05056	108.21	1→4 H rearrangement
B3003	**E(3)(00)(3)**	**60.4**	**−222.26235**	**−449.44**	2 NH_3 + N_2
C2211	E(22)(11)d	12.3	−222.10759	−41.45	H_2N-NH_2 + HN=NH
C2202	E(22)(02)	29.6	−222.07822	35.58	H_2N-NH_2 + N=NH_2
C2121	E1111	23.1	−221.99631	250.64	Cyclo-N_4H_4 + H_2

In the case of cyclo-N_4H_6 isomers we can use the same notation, but any N-N fission can lead to $^{15}N^{14}N$ molecules because of suitable H transfers within the cycle.

We introduce the notation Xmnpq for the individual systems under study, where X = A, B and C, and D stands for anti-, syn-, cyclic and gauche-structures and the indices m, n, p and q are explained above. X = E denotes structures with N-N fissions, i.e., consisting of two or three molecules after geometry optimization. X = F stands for structures with N2-N3 fissions and subsequent N1-N4 bond formations. The N-N fissions in E and F systems are denoted by round brackets where the mutually bonded N atoms are included in the same bracket couple. The different structures with the same Xmnpq notation can be distinguished by additional letters a, b, c, etc. For example, E(22)(11)a and E(22)(11)b denote two different structures composed of H_2N-NH_2 and HN=NH molecules.

The N_4H_6 structures under study are shown in Table 2 and are divided into three groups according to the initial N1-N2-N3-N4 conformations. The H atom rearrangements during geometry optimizations are less frequent in the anti-conformations (starting A structures) than in the syn-conformations (starting B structures). In both groups the probability of N-N fissions is approximately 50%, and N2-N3 fissions prevail. On the other hand, the N1-N2 fissions lead to energetically preferred products such as E(3)(201), E(3)(102) and especially E(3)(00)(3). In the B1221 syn-conformation the mutual interaction of N1 and N4 causes the formation of the N1-N4 bond and N2-N3 fission leading to the structure of H_2N2-N1H-N4H-N3H_2, i.e., F12)(21, in gauche conformation or decomposition to more stable HN1=N4H and H_2N2-N3H_2 species denoted as the F1)(22)(1 system.

The relative Gibbs free energies in Table 2 are related to the structure D2112a obtained by the reaction (6) in the first step. According to these data, the system E(3)(00)(3), which corresponds to $^{15}NH_3$, $^{14}NH_3$ and $^{15}N^{14}N$ molecules, is dominant among all N_4H_6 structures in aqueous solutions under normal conditions and the relative abundance of the remaining systems vanishes. In general, the decomposed E systems are more stable than the remaining structures (see Tables 2–4, Figures 1 and 2).

Table 3. Interatomic distances (in Å) in the optimized Amnpq and Dmnpq structures. The different structures with the same notation are distinguished by additional letters a, b, c, or d.

Structure	N1-N2	N2-N3	N3-N4	N1-H	N2-H	N3-H	N4-H
D1221	1.341	1.840	1.338	1.017	1.019 1.016	1.015 1.021	1.018
D2112a	1.423	1.467	1.431	1.012 1.018	1.014	1.016	1.011 1.014
D2112b	1.432	1.419	1.440	1.012 1.015	1.018	1.013	1.011 1.015
D2112c	1.424	1.428	1.437	1.013 1.017	1.016	1.014	1.011 1.015
D2121a	1.413	1.480	1.412	1.011 1.017	1.015	1.020 1.021	1.018
D2121b	1.423	1.467	1.417	1.010 1.013	1.018	1.017 1.020	1.019

Table 3. *Cont.*

Structure	N1-N2	N2-N3	N3-N4	N1-H	N2-H	N3-H	N4-H
D2121c	1.413	1.504	1.409	1.013 1.024	1.017	1.017 1.020	1.020
D2121d	1.423	1.467	1.415	1.010 1.013	1.018	1.016 1.021	1.018
A2202	1.427	1.454	1.443	1.016(2×)	1.021(2×)	-	1.013(2×)
D2202a	1.459	1.422	1.446	1.017(2×)	1.016 1.022	-	1.012 1.013
D2202b	1.464	1.418	1.446	1.016 1.018	1.017 1.021	-	1.012 1.014
D2022	1.459	1.421	1.447	1.017(2×)	-	1.016 1.022	1.012 1.013
A3021	1.463	1.452	1.433	1.016 1.024(2×)	-	1.020 1.025	1.019
D3012a	1.463	1.418	1.463	1.016 1.021(2×)	-	1.013	1.015 1.017
D3012b	1.493	1.395	1.485	1.014 1.021(2×)	-	1.021	1.014 1.017

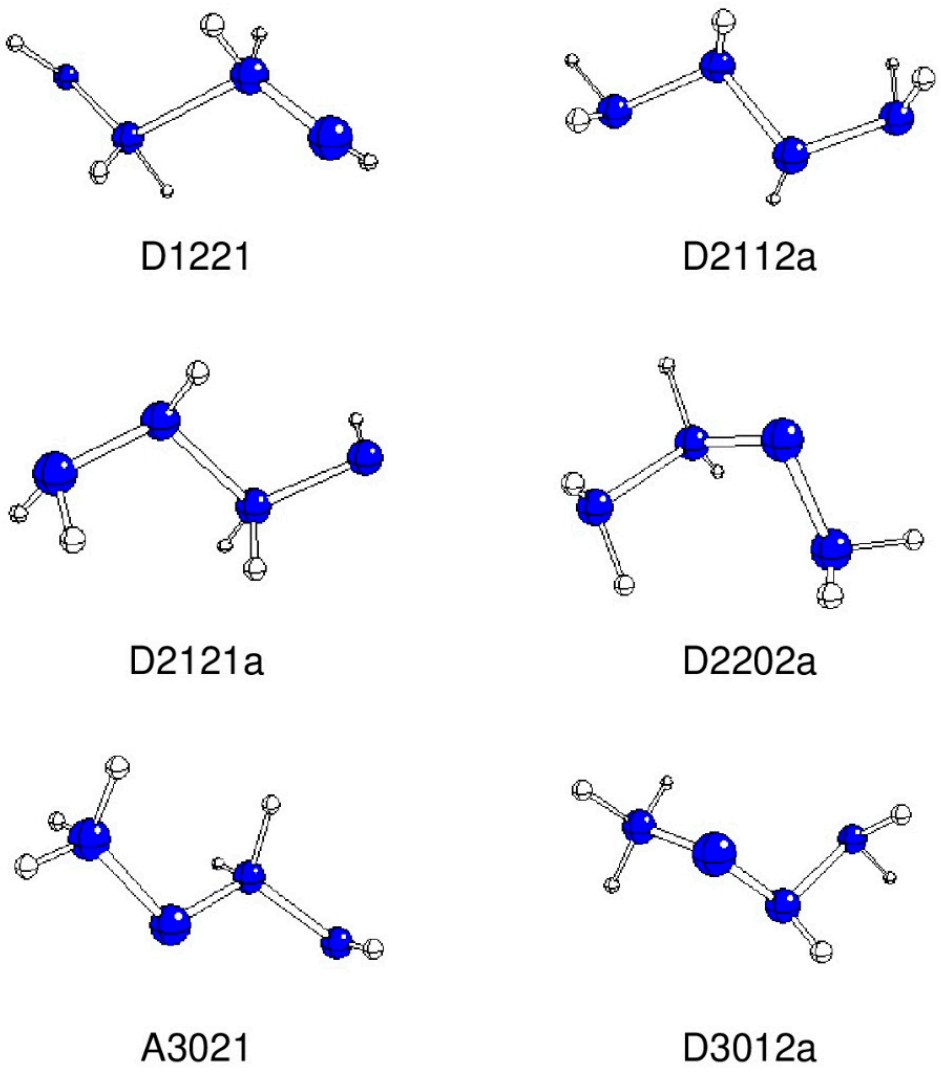

Figure 1. Optimized geometries of stable A and D structures (N—blue, H—white).

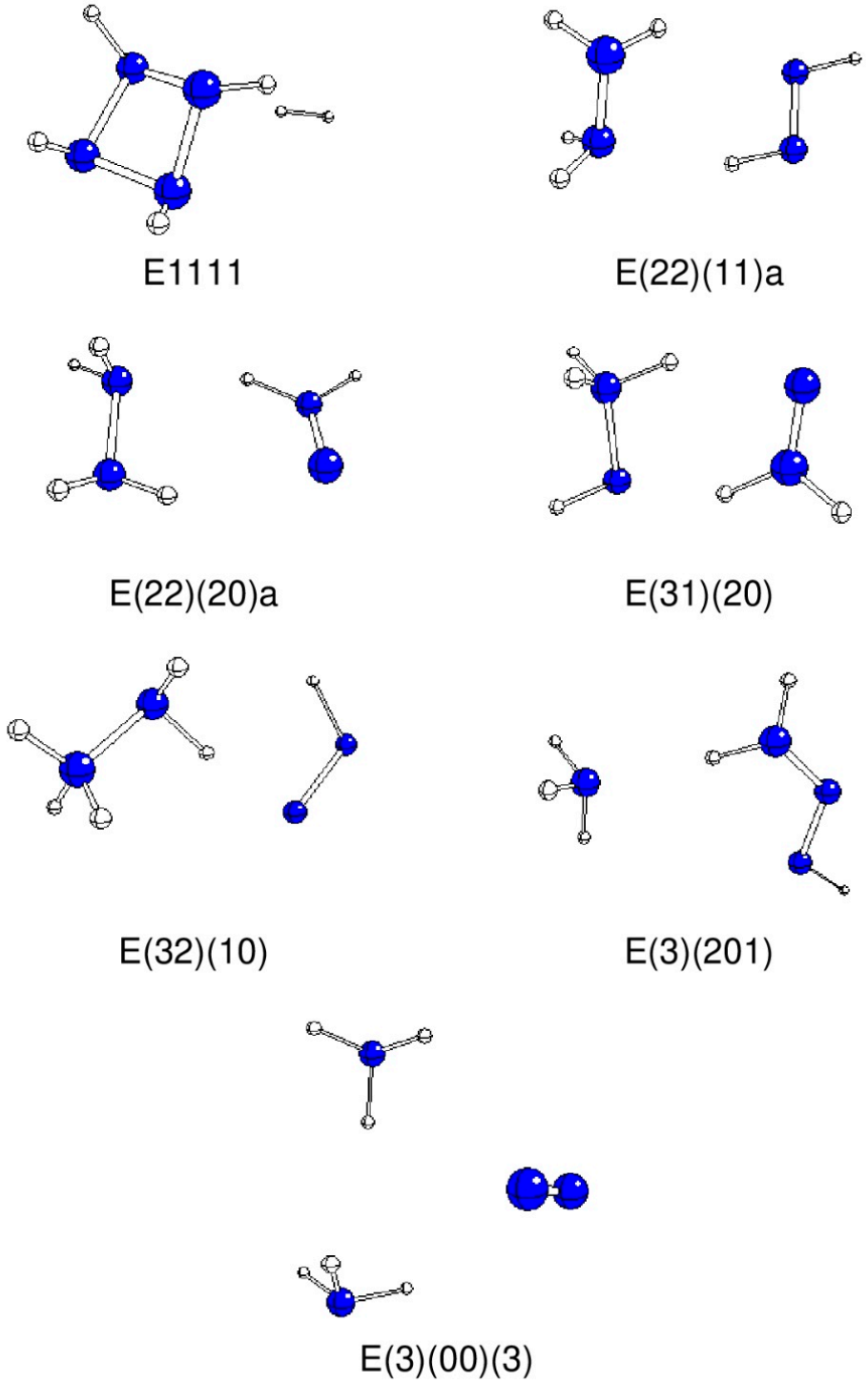

Figure 2. Optimized geometries of stable E systems (N—blue, H—white).

Table 4. Interatomic distances (in Å) in the optimized Emnpq and Fmnpq systems. The different structures with the same notation are distinguished by additional letters a, b, c, or d.

System	N1-N2	N2-N3	N3-N4	N1-H	N2-H	N3-H	N4-H
E1111 [(a)]	1.476	1.481	1.481	1.023	1.017	1.017	1.017
E(22)(11)a	1.446	3.118	1.245	1.012 1.014	1.011 1.014	1.030	1.027

Table 4. *Cont.*

System	N1-N2	N2-N3	N3-N4	N1-H	N2-H	N3-H	N4-H
E(22)(11)b	1.446	3.465	1.245	1.011 1.014	1.012 1.014	1.030	1.027
E(22)(11)c	1.445	3.292	1.245	1.011 1.014	1.012 1.014	1.027	1.030
E(22)(11)d	1.446	3.116	1.245	1.012 1.014	1.011 1.014	1.030	1.027
E(22)(20)a	1.446	3.271	1.225	1.011 1.014	1.013 1.014	1.028 1.034	-
E(22)(20)b	1.446	2.971	1.225	1.013 1.014	1.011 1.014	1.028 1.033	-
E(22)(02)	1.447	3.276	1.225	1.011 1.014	1.013 1.014	-	1.028 1.033
E(31)(20)	1.468	2.750	1.230	1.018(2×) 1.029	1.016	1.029 1.057	-
E(32)(10)	1.445	3.035	1.242	1.018(2×) 1.021	1.015 1.079	1.076	-
E(3)(201)	3.088	1.350	1.249	1.013(3×)	1.006 1.022	-	1.019
E(3)(102)a	3.117	1.243	1.365	1.013(3×)	1.026	-	1.008 1.014
E(3)(102)b	3.760	1.246	1.356	1.013(2×) 1.014	1.032	-	1.007 1.024
E(3)(00)(3)	3.636	1.096	3.711	1.014(3×)	-	-	1.013(3×)
F(11)(22)	1.245	3.291	1.446	1.030	1.027	1.012 1.014	1.011 1.014
F12)(21 [(b)]	1.430	3.017	1.424	1.012	1.012 1.018	1.012 1.017	1.017

Remarks: [(a)] N1-N4 bond length of 1.476 Å, [(b)] N1-N4 bond length of 1.432 Å.

During the geometry optimization of the starting cyclic C structures (Table 2), only the least stable cyclo-$(NH)_4$ structure, denoted as E1111, preserves its tetraatomic ring after removing an H_2 molecule. The remaining C structures split into hydrazine and HN=NH in E(22)(11)d or H_2N=N in E(22)(02). The disadvantage of cyclic structure preservation is indicated by preferring the above-mentioned F structures after N1-N4 bonding within geometry optimization of the starting B1221 syn-conformation.

The bonding within N_4H_6 structures can be described by individual bond lengths *d* (Tables 3 and 4) as well as by the corresponding electron density ρ (Tables 5 and 6) and ellipticity ε (Tables 7 and 8) at their bond-critical points (BCP) [9]. Bond strengths decrease with bond lengths *d* and increase with their BCP electron densities ρ_{BCP}. Their double bond character in acyclic structures increases with their BCP ellipticities ε_{BCP}.

Table 5. BCP electron density (in e/Bohr^3) of N-N and N-H bonds in the optimized Amnpq and Dmnpq structures. The different structures with the same notation are distinguished by additional letters a, b, c, or d.

Structure	N1-N2	N2-N3	N3-N4	N1-H	N2-H	N3-H	N4-H
D1221	0.3705	0.1281	0.3734	0.3450	0.3483 0.3528	0.3467 0.3534	0.3448
D2112a	0.3156	0.2911	0.3092	0.3459 0.3515	0.3574	0.3551	0.3492 0.3518
D2112b	0.3092	0.3237	0.3036	0.3494 0.3508	0.3527	0.3561	0.3484 0.3514

Table 5. *Cont.*

Structure	N1-N2	N2-N3	N3-N4	N1-H	N2-H	N3-H	N4-H
D2112c	0.3149	0.3165	0.3050	0.3472 0.3513	0.3542	0.3552	0.3484 0.3515
D2121a	0.3212	0.2827	0.3080	0.3458 0.3516	0.3544	0.3520 0.3527	0.3415
D2121b	0.3149	0.2920	0.3074	0.3509 0.3517	0.3524	0.3521 0.3551	0.3404
D2121c	0.3224	0.2668	0.3133	0.3406 0.3505	0.3542	0.3508 0.3556	0.3404
D2121d	0.3149	0.2928	0.3086	0.3503 0.3521	0.3523	0.3509 0.3559	0.3417
A2202	0.3148	0.2864	0.2965	0.3478(2×)	0.3514(2×)	-	0.3504 0.3503
D2202a	0.2928	0.3098	0.2951	0.3469 0.3474	0.3499 0.3553	-	0.3506(2×)
D2202b	0.2898	0.3107	0.2956	0.3447 0.3478	0.3507 0.3549	-	0.3501 0.3510
D2022	0.2949	0.3102	0.2930	0.3505 0.3507	-	0.3498 0.3552	0.3470 0.3474
A3021	0.2759	0.2964	0.2956	0.3431 0.3437 0.3480	-	0.3499 0.3542	0.3397
D3012a	0.2761	0.3196	0.2874	0.3454 0.3473 0.3500	-	0.3564	0.3463 0.3476
D3012b	0.2562	0.3362	0.2736	0.3446 0.3450 0.3501	-	0.3488	0.3455 0.3497

Table 6. BCP electron density (in e/Bohr^3) of N-N and N-H bonds in the optimized Emnpq and Fmnpq systems. The different structures with the same notation are distinguished by additional letters a, b, c, or d.

System	N1-N2	N2-N3	N3-N4	N1-H	N2-H	N3-H	N4-H
E1111 [(a)]	0.2858	0.2828	0.2824	0.3506	0.3545	0.3566	0.3546
E(22)(11)a	0.2953	-	0.4863	0.3502 0.3529	0.3500 0.3529	0.3463	0.3483
E(22)(11)b	0.2953	-	0.4826	0.3500 0.3529	0.3502 0.3529	0.3462	0.3482
E(22)(11)c	0.2954	-	0.4863	0.3500 0.3529	0.3503 0.3529	0.3482	0.3462
E(22)(11)d	0.2953	-	0.4863	0.3502 0.3529	0.3500 0.3529	0.3463	0.3482
E(22)(20)a	0.2947	-	0.4970	0.3499 0.3529	0.3501 0.3518	0.3367 0.3422	-
E(22)(20)b	0.2945	-	0.4967	0.3501 0.3517	0.3499 0.3529	0.3367 0.3423	-
E(22)(02)	0.2945	-	0.4967	0.3500 0.3529	0.3501 0.3517	-	0.3367 0.3423
E(31)(20)	0.2696	-	0.4927	0.3382 0.3486 0.3493	0.3426	0.3123 0.3412	-
E(32)(10)	0.2929	-	0.4831	0.3471 0.3453 0.3474	0.2909 0.3485	0.3032	-

Table 6. *Cont.*

System	N1-N2	N2-N3	N3-N4	N1-H	N2-H	N3-H	N4-H
E(3)(201)	-	0.3794	0.4825	0.3434 0.3435 0.3436	0.3531 0.3368	-	0.3503
E(3)(102)a	-	0.4891	0.3669	0.3435(2×) 0.3436	0.3448	-	0.3457 0.3521
E(3)(102)b	-	0.4833	0.3719	0.3432 0.3435 0.3436	0.3375	-	0.3345 0.3523
E(3)(00)(3)	-	0.7140	-	0.3432 0.3433 0.3433	-	-	0.3435 0.3437 0.3442
F(11)(22)	0.4863	-	0.2954	0.3463	0.3482	0.3502 0.3529	0.3500 0.3529
F12)(21 [(b)]	0.3096	-	0.3150	0.3573	0.3451 0.3515	0.3470 0.3515	0.3522

Remarks: [(a)] N1-N4 BCP electron density of 0.2858 e/Bohr^3, [(b)] N1-N4 BCP electron density of 0.3134 e/Bohr^3.

Table 7. BCP ellipticity of N-N and N-H bonds in the optimized Amnpq and Dmnpq structures. The different structures with the same notation are distinguished by additional letters a, b, c, or d.

Structure	N1-N2	N2-N3	N3-N4	N1-H	N2-H	N3-H	N4-H
D1221	0.230	0.107	0.231	0.048	0.015 0.017	0.015 0.016	0.047
D2112a	0.003	0.149	0.024	0.045 0.050	0.041	0.036	0.046 0.051
D2112b	0.040	0.039	0.012	0.046 0.051	0.043	0.051	0.047 0.051
D2112c	0.027	0.046	0.015	0.044 0.047	0.047	0.050	0.046 0.050
D2121a	0.027	0.123	0.198	0.048 0.051	0.046	0.007 0.009	0.073
D2121b	0.035	0.070	0.182	0.045 0.049	0.034	0.011 0.015	0.074
D2121c	0.026	0.074	0.192	0.039 0.048	0.038	0.013(2×)	0.071
D2121d	0.025	0.069	0.178	0.045 0.050	0.033	0.012 0.013	0.073
A2202	0.060	0.302	0.089	0.036(2×)	0.008(2×)	-	0.055(2×)
D2202a	0.045	0.288	0.084	0.034 0.035	0.012 0.013	-	0.053(2×)
D2202b	0.086	0.301	0.087	0.039 0.041	0.010 0.082	-	0.052 0.053
D2022	0.084	0.288	0.046	0.052 0.053	-	0.012 0.013	0.034 0.035
A3021	0.268	0.222	0.169	0.106 0.108 0.005	-	0.006 0.009	0.079
D3012a	0.267	0.124	0.064	0.006 0.007 0.008	-	0.049	0.044 0.048
D3012b	0.248	0.113	0.123	0.004 0.005(2×)	-	0.051	0.038(2×)

Table 8. BCP ellipticity of N-N and N-H bonds in the optimized Emnpq and Fmnpq systems. The different structures with the same notation are distinguished by additional letters a, b, c, or d.

System	N1-N2	N2-N3	N3-N4	N1-H	N2-H	N3-H	N4-H
E1111 [(a)]	0.103	0.108	0.108	0.029	0.030	0.027	0.030
E(22)(11)a	0.008	-	0.189	0.047 0.049	0.046 0.050	0.004	0.004
E(22)(11)b	0.008	-	0.189	0.046 0.050	0.047 0.049	0.004	0.004
E(22)(11)c	0.008	-	0.189	0.046 0.050	0.047 0.049	0.004	0.004
E(22)(11)d	0.008	-	0.189	0.047 0.049	0.046 0.049	0.004	0.004
E(22)(20)a	0.008	-	0.021	0.046 0.049	0.047(2×)	0.035 0.038	-
E(22)(20)b	0.007	-	0.020	0.047(2×)	0.046 0.049	0.035 0.038	-
E(22)(02)	0.007	-	0.020	0.046 0.049	0.047(2×)	-	0.035 0.039
E(31)(20)	0.156	-	0.005	0.006 0.011 0.012	0.080	0.029 0.035	-
E(32)(10)	0.089	-	0.072	0.009 0.010(2×)	0.027 0.045	0.005	-
E(3)(201)	-	0.138	0.229	0.033(3×)	0.043 0.053	-	0.008
E(3)(102)a	-	0.218	0.118	0.326 0.327(2×)	0.005	-	0.047 0.051
E(3)(102)b	-	0.238	0.133	0.324(2×) 0.329	0.001	-	0.041 0.052
E(3)(00)(3)	-	0.000	-	0.033 0.034(2×)	-	-	0.033(3×)
F(11)(22)	0.189	-	0.008	0.004	0.004	0.047 0.049	0.046 0.050
F12)(21 [(b)]	0.012	-	0.031	0.054	0.046 0.051	0.045 0.047	0.049

Remarks: [(a)] N1-N4 BCP ellipticity of 0.103; [(b)] N1-N4 BCP ellipticity of 0.041.

The D1221 structure has an extremely long N2-N3 bond, and the remaining N-N bonds are shorter than the average N_4H_6 ones. The ρ_{BCP}(N2-N3)~0.1 e/Bohr^3 corresponds to a very weak bond, and the remaining N-N bonds are approximately three times stronger. The ε_{BCP}(N2-N3)~0.1 is relatively high, and the remaining double N-N bonds have a ca. two times higher ellipticity.

The D2112a-c structures differ in N1-N2-N3-N4 dihedral angles, and their bond length alternation decreases with non-planarity of their backbone. Their ρ_{BCP}(N-N) values vary by about ~0.3 e/Bohr^3, as in single N-N bonds. The ε_{BCP}(N2-N3) values decrease with non-planarity (~0.1 and less), while they are very small for the remaining N-N bonds, which correspond to single bonds.

Similarly, the D2121a-d structures differ in the N1-N2-N3-N4 dihedral angles, with the N2-N3 bond length being longer and weaker than the remaining ones'. The ρ_{BCP}(N-N) values that vary by about ~0.3 e/Bohr^3 correspond to single N-N bonds. The ε_{BCP}(N2-N3) values decrease with non-planarity (~0.1 and less); ε_{BCP}(N3-N4)~0.2 is typical for double bonds.

The N-N bond properties in the A2202, D2202a-b and D2022 structures (aside from reverse numbering of N atoms) vary with the N1-N2-N3-N4 dihedral angles. The N2-N3 bonds are the shortest in all these systems. The ρ_{BCP}(N-N) values that vary by about ~0.3 e/Bohr^3 are typical for single N-N bonds but the ε_{BCP}(N2-N3)~0.3 in all structures indicate the double-bond character of this bond.

In A3021 the N-N bond lengths decrease with the distance from N1, and the BCP ellipticity values indicate the same trend in decreasing double-bond character. However, the ρ_{BCP}(N-N) values of about 0.3 e/Bohr^3 correspond to single N-N bonds.

Analogous trends are observed for D3012a-b structures.

In E1111 with N-N bond lengths of ca. 1.5 Å and ρ_{BCP}(N-N)~0.3 e/Bohr^3 typical for single N-N bonds, the ε_{BCP}(N-N) values of 0.108 can be explained by mechanical strain in its four-membered ring rather than by its double-bond character.

The remaining E systems consist of two or three independent molecules, interacting through weak hydrogen bonds only, which can be treated independently of their parent E structures. The possible biradical character of E(32)(10) can be excluded on the basis of its atomic charges (see later) which indicate the existence of $[NH_3\text{-}NH_2]^+$ and $[HN{\equiv}N]^-$ charged species.

$H_2N\text{-}NH_2$ with an N-N distance of 1.45 Å, ρ_{BCP}(N-N) = 0.295 e/Bohr^3 and ε_{BCP}(N-N) = 0.008 in all E systems is typical for a single N-N bond.

HN=NH with an N-N distance of 1.245 Å, ρ_{BCP}(N-N) = 0.486 e/Bohr^3 and ε_{BCP}(N-N) = 0.189 in all E systems corresponds to the double N-N bond.

Its isomer $H_2N{=}N$ has a N-N distance of 1.23 Å and ρ_{BCP}(N-N) = 0.497 e/Bohr^3 which correspond to the double N-N bond in contradiction with ε_{BCP}(N-N) = 0.020, which corresponds to single or triple bonds.

On the other hand, $NH_3\text{-}NH$ has a N-N distance of 1.47 Å and ρ_{BCP}(N-N) = 0.27 e/Bohr^3, which corresponds to the single N-N bond in contrast to the high ε_{BCP}(N-N) value of 0.156.

The $[NH_3\text{-}NH_2]^+$ cation with an N-N distance of 1.446 Å, ρ_{BCP}(N-N) = 0.293 e/Bohr^3 and ε_{BCP}(N-N) = 0.089 corresponds to a single N-N bond.

Its counterpart $[HN{\equiv}N]^-$ has a N-N distance of 1.242 Å and ρ_{BCP}(N-N) = 0.48 e/Bohr^3 which correspond to the double N-N bond in contradiction with its too low ε_{BCP}(N-N) = 0.072.

N_2 has a N-N distance of 1.096 Å, ρ_{BCP}(N-N) = 0.714 e/Bohr^3 and ε_{BCP}(N-N) = 0.000, which is typical for the triple bond.

Finally, $H_2N\text{-}N{=}NH$ with N-N distances of 1.36 and 1.24 Å, ρ_{BCP}(N-N) values of 0.37 and 0.48 e/Bohr^3 as well as ε_{BCP}(N-N) values of 0.23 and 0.13, respectively, probably correspond to nearly-double N-N bonds.

The F(11)(22) system is explained within the $HN{\equiv}NH$ and $H_2N\text{-}NH_2$ structures above.

The F12)(21 structure $H_2N2\text{-}N1H\text{-}N4H\text{-}N3H_2$ (aside from different numbering of N atoms) corresponds to the D2112 structures explained above.

We have not discussed N-H bonding in the systems under study because the differences in their bond lengths and BCP electron densities are too small. However, their BCP electron densities are higher than those of N-N bonds except HN=NH, $H_2N{=}N$, $[HN{\equiv}N]^-$ and N_2. Increased ε_{BCP}(N-H) values can mostly be ascribed to the double-bond character of neighboring N-N bonds, except ε_{BCP}(N-H) = 0.3 in NH_3 molecules within the E(3)(102) systems.

The nitrogen atomic charges in the A and D structures (Table 9) on the N1 and N4 atoms are more negative (−0.65 to −0.82) than on the central N2 and N3 atoms (−0.35 to −0.50). Positive hydrogen atomic charges bonded to side N1 and N4 atoms increase with the number of bonded H atoms. The same trend holds for H atoms bonded to central N2 and N3 atoms which are more positive than the side hydrogens.

In the decomposed E systems (Table 10), negative N charges increase with the number of bonded H atoms. An analogous trend for positive H charges cannot be confirmed. Atomic charges are only slightly affected by hydrogen bonding. In the E(32)(10) system, the charges of its $[NH_3\text{-}NH_2]^+$ and $[HN{\equiv}N]^-$ subsystems are +0.97 and −0.68, respectively (the ideal charges are +1.00 and −1.00, respectively). The errors can be ascribed to numerical integration of electron density up to 0.001 e/Bohr^3 (instead of 0.000 e/Bohr^3). A significantly higher error of $[HN{\equiv}N]^-$ is caused by the higher diffusive character of the electron density of anionic species. When accounting for the errors in the electron density

integration over atomic basins, the alternative biradical structure of the neutral E(32)(10) subsystems (the ideal charges of both species should be 0.00) seems to be less probable.

Table 9. Atomic charges of N and H (bonded to N in brackets) in the optimized Amnpq and Dmnpq structures. The asterisks denote the atoms also included in hydrogen bonds. The different structures with the same notation are distinguished by additional letters a, b, c, or d.

Structure	N1	N2	N3	N4	H(N1)	H(N2)	H(N3)	H(N4)
D1221	−0.657	−0.488	−0.485	−0.649	0.342	0.452 0.455	0.444 0.457	0.342
D2112a	−0.699	−0.347	−0.367	−0.706	0.379 0.392	0.391	0.382	0.391 0.404
D2112b	−0.691	−0.357	−0.354	−0.726	0.378 0.394	0.372	0.395	0.387 0.398
D2112c	−0.711	−0.354	−0.368	−0.729	0.377 0.389	0.382	0.396	0.389 0.401
D2121a	−0.700	−0.341	−0.398	−0.787	0.394 0.413	0.417	0.452(2×)	0.309
D2121b	−0.704	−0.361	−0.394	−0.811	0.400 0.416	0.405	0.470 0.560	0.302
D2121c	−0.709	−0.365	−0.412	−0.800 *	0.396 0.407 *	0.406	0.463 0.468	0.310
D2121d	−0.707	−0.361	−0.395	−0.809	0.402 0.420	0.408	0.458 0.471	0.304
A2202	−0.664	−0.388	−0.435	−0.750	0.418(2×)	0.450(2×)	-	0.362(2×)
D2202a	−0.712	−0.404	−0.430	−0.760	0.409 0.410	0.455 0.475	-	0.361 0.364
D2202b	−0.705	−0.397	−0.432	−0.737	0.407 0.411	0.459 0.465	-	0.357 0.367
D2022	−0.761	−0.430	−0.402	−0.711	0.361 0.365	-	0.455 0.475	0.409 0.410
A3021	−0.730	−0.368	−0.388	−0.824	0.460 0.461 0.496	-	0.403 0.423	0.286
D3012a	−0.732	−0.436	−0.390	−0.739	0.449(2×) 0.472	-	0.370	0.360 0.372
D3012b	−0.762	−0.417	−0.384	−0.754 *	0.444 0.466 * 0.473	-	0.345	0.376 0.378

Table 10. Atomic charges of N and H (bonded to N in bracket) in the optimized Emnpq and Fmnpq systems. Asterisks denote atoms also included in hydrogen bonds. The different structures with the same notation are distinguished by additional letters a, b, c, or d.

System	N1	N2	N3	N4	H(N1)	H(N2)	H(N3)	H(N4)
E1111	−0.345	−0.367 *	−0.373	−0.367	0.383	0.408	0.396 *	0.403
E(22)(11)a	−0.707	−0.727 *	−0.358	−0.348 *	0.380 0.392 *	0.385 0.393	0.409 *	0.380
E(22)(11)b	−0.727 *	−0.707	−0.360	−0.348 *	0.384 0.393	0.380 0.388 *	0.409 *	0.380
E(22)(11)c	−0.726 *	−0.706	−0.349h	−0.360	0.384 0.393	0.380 0.387 *	0.380	0.409h
E(22)(11)d	−0.706	−0.726 *	−0.359	−0.347 *	0.380 0.388 *	0.384 0.393	0.409 *	0.380
E(22)(20)a	−0.732 *	−0.714	−0.519	−0.271 *	0.380 0.393 *	0.387 0.395	0.417 0.460 *	-
E(22)(20)b	−0.713	−0.732 *	−0.517	−0.273 *	0.380 0.393 *	0.387 0.395	0.417 0.461 *	-

Table 10. *Cont.*

System	N1	N2	N3	N4	H(N1)	H(N2)	H(N3)	H(N4)
E(22)(02)	−0.714	−0.732 *	−0.272 *	−0.517	0.380 0.393 *	0.387 0.395	-	0.417 0.460 *
E(31)(20)	−0.751	−0.831 *	−0.543	−0.306 *	0.447 0.452 0.491 *	0.315	0.408 0.511 *	-
E(32)(10)	−0.718	−0.731	−0.426	−0.530 *	0.496 0.508(2×)	0.408 0.501 *	0.185	-
E(3)(201)	−1.079 *	−0.734	−0.035	−0.436	0.394(3×)	0.443 0.473 *	-	0.388
E(3)(102)a	−1.076 *	−0.454	−0.033	−0.686	0.394(3×)	0.428 *	-	0.429 0.445
E(3)(102)b	−1.084 *	−0.396	−0.030	−0.739	0.394 0.395 0.396	0.352	-	0.445 0.470 *
E(3)(00)(3)	−1.077 *	0.076 *	−0.049	−1.059	0.382 0.382 * 0.384	-	-	0.373 0.380 * 0.386
F(11)(22)	−0.359	−0.347 *	−0.706	−0.725 *	0.409 *	0.380	0.380 0.388 *	0.393 0.394
F12)(21	−0.356	−0.722	−0.702	−0.368	0.403	0.377 0.392	0.371 0.395	0.381

3. Method

Geometry optimizations for various isomers of neutral N_4H_6 molecules were performed at the CCSD (Coupled Cluster using Single and Double substitutions from the Hartree-Fock determinant) [10] level of theory and cc-pVTZ basis sets [11]. The effects of the aqueous solution were taken into account within the SMD (Solvation Model based on the solute electron Density) solvation model [12]. The optimized structures were tested by vibrational analysis for the absence of imaginary vibrations. Gaussian16 (Revision B.01) software [13] was used for all quantum-chemical calculations.

The electron structures of the systems under study were evaluated in terms of Quantum Theory of Atoms-in-Molecules (QTAIM) [9] using AIM2000 (Version 1.0) software [14]. The bond strengths were compared according to the electron densities ρ at the bond-critical points (BCP). The BCP bond ellipticities ε_{BCP} were evaluated as

$$\varepsilon_{BCP} = \lambda_1/\lambda_2 - 1 \quad (7)$$

where λ_i are the eigenvalues of the Hessian of the BCP electron density within the sequence $\lambda_1 < \lambda_2 < 0 < \lambda_3$. Atomic charges were obtained by integration over atomic basins up to 0.001 e/Bohr^3.

Visualization and geometry modification were performed using MOLDRAW (Release 2.0) software (https://www.moldraw.software.informer.com, accessed on 9 September 2019) [15].

4. Conclusions

We have shown that most N_4H_6 structures in aqueous solutions are decomposed during geometry optimization. Splitting the bond between central nitrogen atoms is the most frequent method, but the breakaway of the side nitrogen is energetically the most preferred one. The N-N fissions are enabled by suitable hydrogen rearrangements. The initial H_2N-NH-NH-NH_2 structure (D2112) has a very weak central N-N bond, which explains the high degree of reversibility for the reaction (6). The most stable system NH_3...N_2...NH_3 (E(3)(00)(3) system) might be obtained by transfers of both H atoms bonded with central nitrogens to the side N atoms. According to [8], such double H transfer was not found by quantum-chemical calculations in vacuo, and so must be decomposed into

several steps and this instantaneous decomposition should be slowed down. Furthermore, our calculations show that the transfer of the third H atom to the side nitrogen is very energetically disadvantageous, as indicated by the Gibbs energies of the structures NH_3-N=NH_2-NH and NH_3-N=NH-NH_2 (A3021 and D3012, respectively, see Table 2). In aqueous solutions, H atom transfers can be mediated by H_2O, H_3O^+ and/or OH^- species. We have shown that side N atoms have very high negative charges that should support such hydrogen transfers.

The experimentally observed formation of $^{15}N^{14}N$ molecules [1–4] is enabled by side N-N fissions. We have shown that the Gibbs free energy data (Table 2) indicate the dominant abundance of the NH_3... N_2... NH_3 species (E(3)(00)(3) system) in aqueous solutions, which explains the mentioned observations.

The $^{15}N^{14}N$ molecules can also be created by the decomposition of cyclic N_4H_6 structures. We have shown the high instability of such species. The only stable cyclo-$(NH)_4$...H_2 structure (E1111) has a too-high Gibbs energy and breaks the H_2 molecule instead. The remaining initial cyclic structures are split into hydrazine and HN≡NH (E(22)(11)d) or H_2N≡N species (E(22)(02), see Table 2), and their relative abundance in aqueous solutions vanishes.

We can deduce from the QTAIM analysis of our systems that single, double and triple N-N bonds exhibit BCP electron densities of ca. 0.2, 0.5 and 0.7 e/Bohr^3 with BCP ellipticities of ca 0, 0.2 and 0, respectively. The bonds in the N_4H_6 structures often exhibit significant deviations from these values.

Our study did not solve all of the problems related to hydrazine oxidation in aqueous solutions. The role of various water forms and the corresponding transition states should also be investigated. The transition states can possibly be of extremely high-energy. Thus, the thermodynamic stability of the products means less if their formation is kinetically hindered. Moreover, directly accounting for the solvent molecules is required. An alternative reaction pathway through N_4H_4 [6] according to reaction (5) is worth studying as well. Further theoretical studies in these fields are desirable.

Author Contributions: Methodology, software, investigation, writing—original draft preparation, writing—review and editing, M.B.; conceptualization, supervision, project administration, funding acquisition, A.M. All authors have read and agreed to the published version of the manuscript.

Funding: This publication was supported by the Competence Center for SMART Technologies for Electronics and Informatics Systems and Services under the project no. ITMS 26240220072.

Institutional Review Board Statement: Not applicable.

Informed Consent Statement: Not applicable.

Data Availability Statement: All necessary research data are presented in the article.

Acknowledgments: M.B. thanks the HPC center at the Slovak University of Technology in Bratislava, which is a part of the Slovak Infrastructure of High Performance Computing (SIVVP Project No. 26230120002, funded by the European Region Development Funds), for computing facilities.

Conflicts of Interest: The authors declare no conflict of interest.

References

1. Lauko, L.; Hudec, R.; Lenghartova, K.; Manova, A.; Cacho, F.; Beinrohr, E. Simple Electrochemical Determination of Hydrazine in Water. *Pol. J. Environ. Stud.* **2015**, *24*, 1659–1666. [CrossRef] [PubMed]
2. Higginson, W.C.E.; Sutton, D. The Oxidation of Hydrazine in Aqueous Solution. Part II. The Use of ^{15}N as a Tracer in the Oxidation of Hydrazine. *J. Chem. Soc.* **1953**, 1402–1406. [CrossRef]
3. Cahn, J.W.; Powell, R.E. Oxidation of Hydrazine in Solution. *J. Am. Chem. Soc.* **1954**, *76*, 2568–2572. [CrossRef]
4. Petek, M.; Bruckenstein, S. An Isotopic Labeling Investigation of the Mechanism of the Electrooxidation of Hydrazine at Platinum. An Electrochemical Mass Spectrometric Study. *Electroanal. Chem. Interrac. Electrochem.* **1973**, *47*, 329–333. [CrossRef]
5. Rice, F.O.; Sherber, F. The Hydrazino Radical and Tetrazane. *J. Am. Chem. Soc.* **1955**, *77*, 291–293. [CrossRef]
6. Karp, S.; Meites, L. The Voltammetric Characteristics and Mechanism of Electrooxidation of Hydrazine. *J. Am. Chem. Soc.* **1962**, *84*, 906–912. [CrossRef]

7. Ball, D.W. Tetrazane: Hartree-Fock, Gaussian-2 and -3, and Complete Basis Set Predictions of Some Thermochemical Properties of N_4H_6. *J. Phys. Chem. A* **2001**, *105*, 465–470. [CrossRef]
8. Dana, A.G.; Moore, K.B., III; Jasper, A.W.; Green, W.H. Large Intermediates in Hydrazine Decomposition: A Theoretical Study of the N_3H_5 and N_4H_6 Potential Energy Surfaces. *J. Phys. Chem. A* **2019**, *123*, 4679–4692. [CrossRef] [PubMed]
9. Bader, R.F.W. *Atoms in Molecules: A Quantum Theory*; Clarendon Press: Oxford, UK, 1990; ISBN 9780198558651.
10. Scuseria, G.E.; Janssen, C.L.; Schaefer, H.F., III. An efficient reformulation of the closed-shell coupled cluster single and double excitation (CCSD) equations. *J. Chem. Phys.* **1988**, *89*, 7382–7387. [CrossRef]
11. Dunning, T.H., Jr. Gaussian basis sets for use in correlated molecular calculations. I. The atoms boron through neon and hydrogen. *J. Chem. Phys.* **1989**, *90*, 1007–1023. [CrossRef]
12. Marenich, A.V.; Cramer, C.J.; Truhlar, D.G. Universal solvation model based on solute electron density and a continuum model of the solvent defined by the bulk dielectric constant and atomic surface tensions. *J. Phys. Chem. B* **2009**, *113*, 6378–6396. [CrossRef] [PubMed]
13. Frisch, G.W.; Trucks, M.J.; Schlegel, H.B.; Scuseria, G.E.; Robb, M.A.; Cheeseman, J.R.; Scalmani, G.; Barone, V.; Petersson, G.A.; Nakatsuji, H.; et al. *Gaussian 16, Revision B.01*; Gaussian, Inc.: Wallingford, CT, USA, 2016.
14. Biegler-König, F.; Schönbohm, J.; Bayles, D. AIM2000—A Program to Analyze and Visualize Atoms in Molecules. *J. Comput. Chem.* **2001**, *22*, 545–559.
15. Ugliengo, P. MOLDRAW: A Program to Display and Manipulate Molecular and Crystal Structures, University Torino, Torino. 2012. Available online: https://www.moldraw.software.informer.com (accessed on 9 September 2019).